ChemPubSoc Europe

DOI: 10.1002/cbic.201900061

CHEMBIOCHEM Communications

Artificial Cellulosome Complex from the Self-Assembly of Ni-NTA-Functionalized Polymeric Micelles and Cellulases

Lin Lu[+,[a]] Libo Zhang[+,[a]] Liang Yuan,[a] Tianyu Zhu,[a] Wilfred Chen,[b] Guiren Wang,[c] and Qian Wang*[a]

Polymer–protein core–shell nanoparticles have been explored for enzyme immobilization. This work reports on the development of functional polymeric micelles for immobilizing His_6-tagged cellulases with controlled spatial orientation of enzymes, resulting in "artificial cellulosomes" for effective cellulose hydrolysis. Poly(styrene)-*b*-poly(styrene-*alt*-maleic anhydride) was prepared through one-pot reversible addition–fragmentation chain-transfer polymerization and modified with nitrilotriacetic acid (NTA) to afford an amphiphilic block copolymer. The self-assembled polymer was mixed with a solution of $NiSO_4$ to form Ni-NTA-functionalized micelles, which could successfully capture His_6-tagged cellulases and form hierarchically structured core–shell nanoparticles with cellulases as the corona. Because the anchored enzymes are site-specifically oriented and in close proximity, synergistic catalysis that results in over twofold activity enhancement has been achieved.

As an emerging research area, one challenge of using proteins in bioengineering and biocatalysis is to control the protein orientation, while maintaining its folding conformation and activity. For many applications, it is necessary to have multiple proteins organized spatially to afford synergy in biological functions. As a natural example, the cellulosome is mainly composed of a cellulose binding module (CBM) and several repeating cohesin domains, which are docked individually to different cellulases tagged with the corresponding dockerin domains (Figure 1 A).[1] Due to the highly ordered architecture, the assembled multiple enzymes are in close proximity to each other and allow highly efficient hydrolysis through synergistic catalysis of multiple cellulases. However, native cellulosome is impractical for use in large-scale biomass hydrolysis because the full-length cellulosome is structurally fragile and cannot be recycled.[2] Thus, many attempts have been devoted to the development of artificial cellulosomes to improve accessibility, stability, and catalytic efficiency. As reported in the literature, selected cellulases have been immobilized on certain substrates, including chimeric scaffolds,[3] yeast cells,[4] DNA double helix,[5] quantum dots,[6] and magnetic nanoparticles,[7] to mimic native cellulosome structures with enriched local enzyme concentrations and better synergistic effects.

Polymer–protein hybrids combine the merits of synthetic polymers, such as structure and function diversity, with the biological functions of proteins. They have been broadly used in the fields of nanotechnology,[8] biotechnology,[9] and biomedicine.[10] Previous studies in our group involved the use of poly(4-vinylpyridine) (P4VP) or poly(caprolactone-*graft*-pyridine)-*block*-poly(caprolactone) to immobilize proteins on the surface of polymeric nanoparticles for catalysis, antigen display, and targeted drug-delivery applications.[11] However, due to the lack of specific recognition units, it was impossible to optimize the spatial orientation of immobilized proteins, which greatly hampered the application potential of this system. To address this, polymeric micelles grafted with nitrilotriacetic acid moieties on the corona layer were designed herein (Figure 1 B and C). Selected cellulases were expressed with His_6 tags opposite to their catalytic centers, which could coassemble with the polymeric micelles to prepare "artificial cellulosomes" through specific binding between His_6 tags and Ni-NTA units. In this case, the immobilization of cellulases would not hinder the catalytic activities; a manner that mimics affinity binding between dockerin and cohesin in native cellulosome systems (Figure 1 A). In addition, this system enables control of the distribution and synergistic interactions of different types of cellulases, which is critical to optimize the hydrolysis efficiency of cellulose.

As shown in Figure 2 A, a diblock copolymer, poly(styrene)-*block*-poly(styrene-*alt*-maleic anhydride) (PS-*b*-PSMA), was synthesized and modified with amino-NTA units. PS-*b*-PSMA was reported to be prepared through a one-pot reversible addition–fragmentation chain-transfer (RAFT) polymerization reaction.[12] As discussed by Wooley and Harrisson, a block of alternating copolymers (PSMA) could be formed, regardless of the charging monomer ratios.[13] After the complete consumption of MA, the PSMA chains will continue to extend a homopolystyrene block to form PS-*b*-PSMA. In our study, the St/MA/CTA/AIBN ratio was 200:20:1:0.4 (Figure 2 A). The reaction was stopped after 70% conversion of St to achieve a theoretical molecular structure of PS_{120}-*b*-P(St-*alt*-MA)$_{20}$ and an average molecular weight of 16520 g mol^{-1}. The polymer was characterized by means of ^{1}H NMR spectroscopy (Figure S1 A in the

[a] Dr. L. Lu,[+] L. Zhang,[+] Dr. L. Yuan, T. Zhu, Dr. Q. Wang
Department of Chemistry and Biochemistry, University of South Carolina
631 Sumter Street, Columbia, SC 29208 (USA)
E-mail: wang263@mailbox.sc.edu

[b] W. Chen
Department of Chemical and Biomolecular Engineering
University of Delaware
150 Academy Street, Newark, DE 19716 (USA)

[c] G. Wang
Department of Mechanical Engineering, University of South Carolina
301 Main Street, Columbia, SC 29208 (USA)

[+] The authors contributed equally to this work.

Supporting information and the ORCID identification numbers for the authors of this article can be found under https://doi.org/10.1002/cbic.201900061.

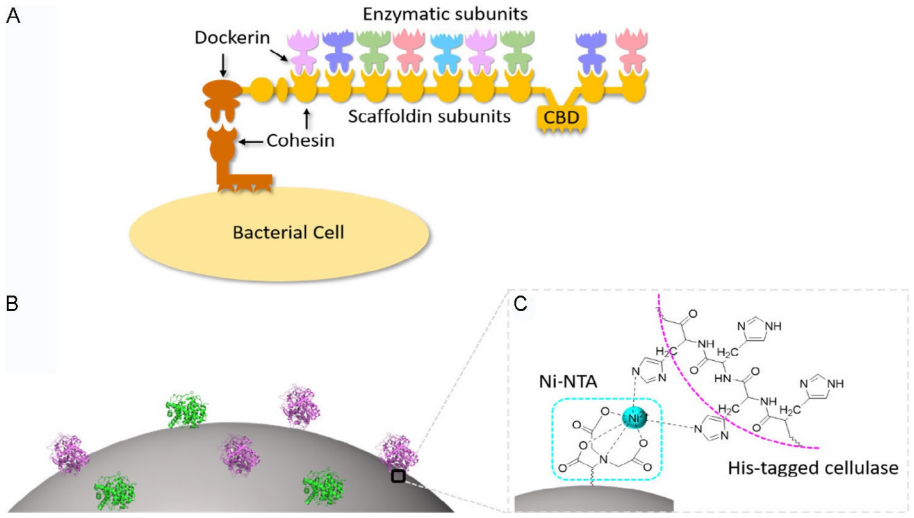

Figure 1. Schematic illustration of A) the structural organization of the cellulosome of *Clostridium thermocellum*, B) Ni-NTA-functionalized micelles for immobilizing cellulases, and C) the interaction of Ni-NTA with His_6-tagged cellulases.

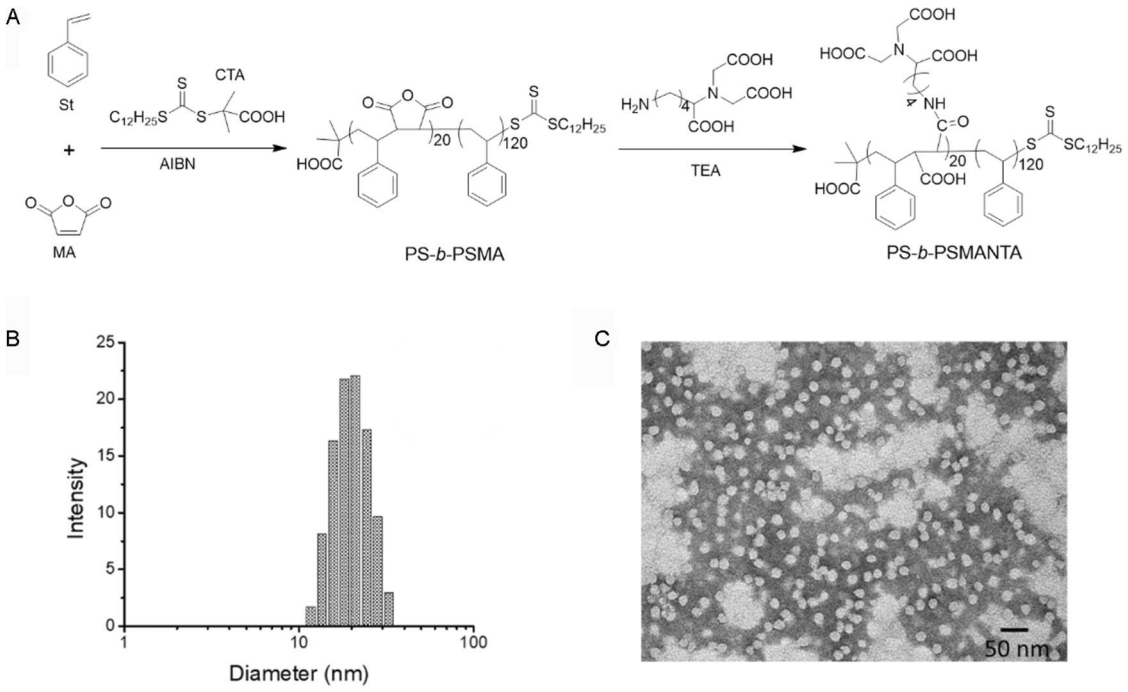

Figure 2. A) Synthetic scheme for the preparation of PS-*b*-PSMANTA. St: styrene, MA: maleic anhydride, AIBN: 2,2′-azobis(isobutyronitrile), CTA: charge transfer agent, TEA: triethylamine. B) dynamic light scattering (DLS) results for PS-*b*-PSMANi-NTA nanoparticles. C) TEM analysis of PS-*b*-PSMANi-NTA nanoparticles; scale bar: 50 nm.

Supporting Information) and gel permeation chromatography (GPC; Figure S1 B). The number-average molecular weight of the polymer was determined to be 13 900 g mol^{-1}, with a polydispersity index ($Đ$) of 1.21 by means of GPC. Differential scanning calorimetry (DSC) characterization (Figure S1 C) showed two distinct glass transition temperatures at 104 and 140 °C; thus supporting that the final product has a block polymer structure.

PS-*b*-PSMA was subsequently modified with amino-NTA to increase the hydrophilicity of the PSMA block. The ratio of amino-NTA to the anhydride group was about 0.38:1. This ratio can be changed based on the targeted grafting density of NTA units. The modified product was characterized by means of ^{1}H NMR (Figure S1 A) and FTIR (Figure S1 D) spectroscopy. The methylene protons next to the amide groups are observed at $\delta = 3.0$ ppm. The appearance of a carboxylic acid absorption band at $\tilde{\nu} = 1725$ cm^{-1} and the decreased anhydride band at $\tilde{\nu} = 1854$ cm^{-1} further proved the modification (Figure S1 D). Core–shell-structured micelles with exposed NTA groups in the shell layer can be obtained from the self-assembly of the NTA-modified polymer. $NiSO_4$ was then added to the solution of micelles to convert NTA into the Ni-NTA complex. DLS indicated

an average size of around 20 nm for the Ni-NTA-functionalized micelles (Figure 2B). The micelles were negatively stained with 2% phosphotungstic acid and observed by TEM, which showed spherical micelles with sizes of around 20–30 nm; this was consistent with DLS results (Figure 2C).

The Ni-NTA complexes on the micelle surfaces are able to capture His_6-tagged proteins and can serve as platforms for constructing new polymer–protein core–shell complexes (Figure 1B). To evaluate the capability of PS-*b*-PSMANi-NTA micelles for capturing His_6-tagged proteins, a model study was performed with expressed His_6-tagged fluorescent proteins, mCherry and enhanced green fluorescent protein (eGFP; Figure S2A). First, mCherry protein was mixed with PS-*b*-PSMANi-NTA particles, with a molar ratio of Ni-NTA to protein of 10:1. Theoretically, each polymer chain has approximately 7.6 Ni-NTA groups, on average. Ideally, the assembled structure will have about one protein on each polymer chain. Fast protein liquid chromatography (FPLC) was used to compare the elution volume of mCherry, bare micelles, and the micelle/mCherry assembly (Figure S3A). Three wavelengths, $\lambda = 254$, 280, and 587 nm, were monitored. The styrene groups have a maximum absorption at $\lambda = 254$ nm, and the mCherry protein has absorption bands at $\lambda = 254$, 280, and 587 nm. The elution volume of bare micelles was about 9 mL, as detected from the absorption band at $\lambda = 254$ nm and the elution volume for mCherry was at about 16.5 mL, as determined from the absorption band at $\lambda = 587$ nm. After their self-assembly, the major peak of elution volume decreased to about 7 mL; this indicated larger resulting assemblies than that of the bare polymeric micelles. Overlap of the absorption bands at $\lambda = 254$ and 587 nm also indicated that mCherry was anchored on the micelles; thus affording mCherry–PS-*b*-PSMANi-NTA assemblies.

The mCherry protein and eGFP are fluorescence resonance energy transfer (FRET) pairs because there is an overlap of the donor eGFP fluorescent emission spectrum with the acceptor mCherry excitation spectrum.[14] We further tested the coassembly of PS-*b*-PSMANi-NTA micelles with a mixture of mCherry and eGFP. The molar ratio of mCherry to eGFP was controlled to be 1:1, and the molar ratio of Ni-NTA to total proteins was 10:1. The coassembly of PS-*b*-PSMANi-NTA and eGFP was prepared as a control group. The eGFP concentration was the same in both groups. Fluorescence images of PS-*b*-PSMANi-NTA–mCherry-eGFP and PS-*b*-PSMANi-NTA–eGFP particles were taken by using a laser scanning confocal microscope, which used a continuous-wave laser, the wavelength and power of which were $\lambda = 477$ nm and 100 μW, respectively (Figure 3). This laser is suitable for exciting eGFP and minimizing the cross-talk signal from mCherry simultaneously. Compared with PS-*b*-PSMANi-NTA–eGFP particles, PS-*b*-PSMANi-NTA–mCherry–eGFP particles showed significant higher intensity at the red (acceptor) channel and lower signal intensity at the green (donor) channel; thus indicating a strong FRET effect between assembled eGFP and mCherry that are within a very close distance to each other on the particle surface.

To demonstrate the synergistic effect with multiple enzymes, two His_6-tagged endoglucanases, CelA and CelF, which could cleave internal β-glycosidic bonds in the cellulose chain, were chosen in our study. CelA and CelF were assembled with PS-*b*-PSMANi-NTA separately. The 20:1 molar ratio of Ni-NTA to cellulase was first attempted to ensure efficient capture of the enzyme by the particles. DLS indicated an average particle size of 38 nm for PS-*b*-PSMANi-NTA–CelA and 41 nm for PS-*b*-PSMANi-NTA–CelF (Figure S4A), which was consistent with TEM and FPLC analyses (Figure S4B and C). The cellulase activity was evaluated by using 0.1% phosphoric acid swollen cellulose (PASC) as the substrate.[15] The reducing sugars produced by the assembled enzyme/polymer core–shell complexes were compared with that of free enzymes by means of a dinitrosalicylic colorimetric method.[16] As shown in Figure 4A, the assembled PS-*b*-PSMANi-NTA–CelA particles produced about twice as much reducing sugar at that of free CelA after incubation for 4 or 24 h. Similarly enhanced activity of CelF was also observed (Figure 4A), which could be attributed to the specific orientation of proteins on the particle surface and active sites exposed to the substrate. The stability of immobilized cellulases were tested. After storage for two weeks at 4 °C or 48 h at

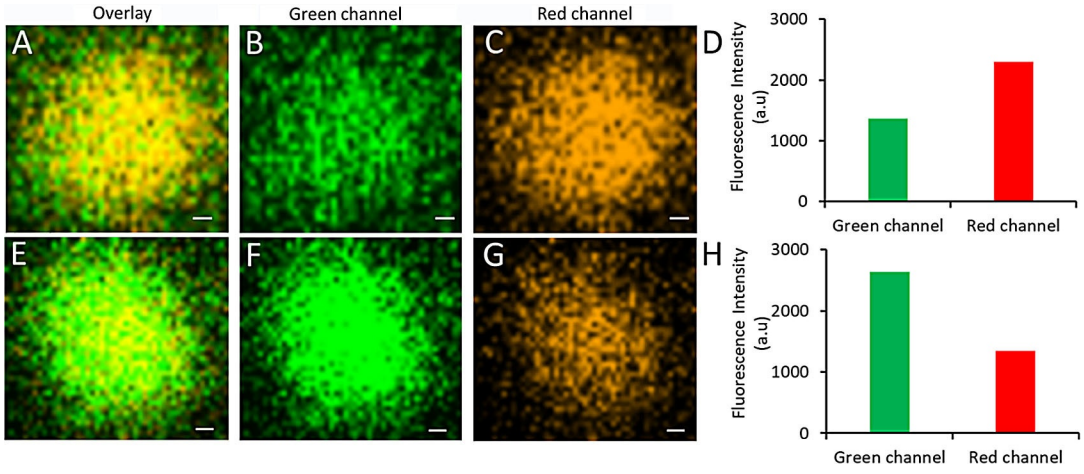

Figure 3. Fluorescence microscopy images and a comparison of the fluorescence intensities at different channels of representative PS-*b*-PSMANi-NTA–mCherry–eGFP (A–D), and PS-*b*-PSMANi-NTA–eGFP (E–H) particles. The laser excitation was at $\lambda = 477$ nm (100 μW). Both channels are represented on the same intensity scale. Overlay images represent a false-color composite of donor (green) and acceptor (red) channels. Scale bar: 100 nm.

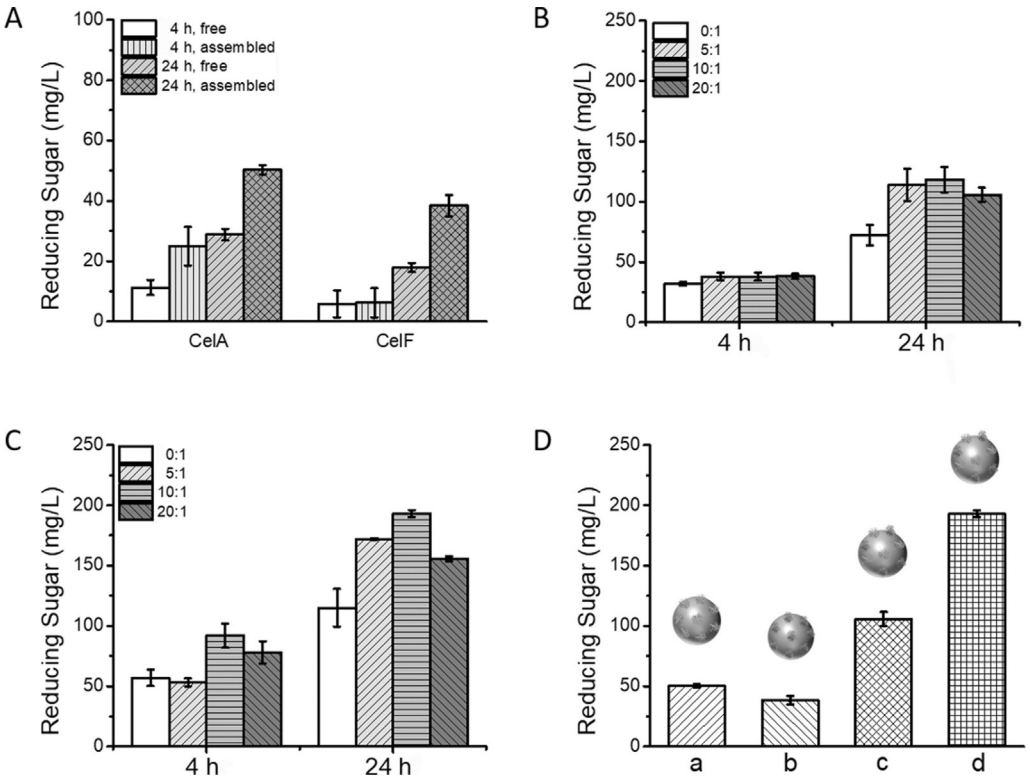

Figure 4. A) Catalytic activity tests of free CelA and assembled CelA (left), and free CelF and assembled CelF (right). The Cel concentration was 1 μM and the molar ratio of Ni-NTA to Cel was 20:1. B), C) Free CelA/CelF mixture and coassembled CelA/CelF. The total Cel concentration was 1 μM in B) and 2 μM in C). D) Activity comparison of a) assembled 1 μM CelA, b) assembled 1 μM CelF, c) coassembled 0.5 μM CelA and 0.5 μM CelF, and d) coassembled 1 μM CelA and 1 μM CelF. The molar ratio of Ni-NTA to Cel was 20:1 in a)–c), and 10:1 in d).

room temperature, the immobilized cellulases did not show significant changes in activity. In a control study, P4VP was assembled with cellulase to form core–shell nanoparticles with cellulases randomly displayed on the surface of the particle. No activity enhancement was observed from these P4VP/cellulase particles (data not shown).

We further studied the synergistic catalysis of CelA and CelF upon coassembly with different molar ratios of Ni-NTA to Cel. A 1:1 molar ratio mixture of CelA and CelF was assembled with the micelles; the molar ratios of Ni-NTA to cellulase mixture were 0:1, 5:1, 10:1, and 20:1. The average particle size decreased from 49 nm (5:1) to 47 (10:1) and 45 nm (20:1; Figure S4A). While keeping the cellulase concentration at 1 μM, the catalytic activities were tested. As shown in Figure 4B, the groups with PS-*b*-PSMANi-NTA particles (5:1, 10:1, 20:1) gave reducing sugar levels 1.5, 1.6, and 1.4 times that of the control group (0:1; free-enzyme mixture) after 24 h. The optimal result was obtained for the 10:1 group, and a higher level of Ni-NTA groups (20:1) led to lower catalytic efficiency. The decreased catalytic effect from the 20:1 group could be attributed to increased spacing between immobilized enzymes. Similar results were observed with a fixed cellulase concentration of 2 μM (Figure 4C).

In native cellulosome, multiple types of cellulases are assembled together through high-affinity docker–cohesin interactions, resulting in the substrate channeling between different enzymes. Therefore, the high efficiency of cellulose hydrolysis is also due to the synergy effect among multiple cellulase units.[2a,17] To demonstrate whether the enhanced catalytic activity of our polymer–enzyme core–shell systems resulted from synergistic interactions between the coassembled enzymes, we quantified the reducing sugar released from 1 μM cellulase after 24 h of reaction (with different compositions of cellulase, at a Ni-NTA to Cel molar ratio of 20:1). As shown in Figure 4D, about 50 mg L^{-1} reducing sugar was produced from the assembled CelA (Figure 4D, a) and 38 mg L^{-1} from the assembled CelF (Figure 4D, b). For comparison, the reducing sugar produced by the 0.5 μM CelA and 0.5 μM CelF coassembled complex was about 106 mg L^{-1} (Figure 4D, c), which was more than twofold that with either CelA or CelF individually. Furthermore, the combined reducing sugar from assembled mono-enzyme CelA (50 mg L^{-1}) and CelF (38 mg L^{-1}) was 88 mg L^{-1} if the molar ratio of Ni-NTA to mono-Cel was 20:1. The coassembled CelA/CelF mixture with a 10:1 ratio of Ni-NTA to Cel produced 193 mg L^{-1} reducing sugar (Figure 4D, d), which was about 2.2-fold activity enhancement, relative to the separately assembled enzymes. The results show that the coassembly of CelA and CelF is essential to achieve higher catalytic activity, and the increase in released reducing sugar is because of both proximity and synergy effects. In another control study, the activity of a mixture of PS-*b*-PSMANTA and CelA/CelF without Ni^{2+} was tested. To minimize the impact of trace amounts of cations from the bacterial culture and cell lysis process, ethylenediaminetetraacetic acid (EDTA) was added to the mixture.

The activity was observed to be similar to that of the CelA/CelF mixture without polymeric support (Table S1); thus proving that our previously observed enhanced activity resulted from Ni^{2+}-assisted enzyme immobilization.

In summary, polymeric nanoparticles with exposed Ni-NTA moieties were prepared to immobilize cellulases for enhanced catalytic activity in hydrolyzing cellulose. PS-*b*-PSMA was prepared through RAFT polymerization in a one-pot method. The anhydride groups in the PSMA block reacted partially with amino-NTA to produce amphiphilic block copolymers. Self-assembly of the NTA-modified polymer in the presence of Ni^{2+} ions formed nanoparticles of about 20 nm in aqueous solution. The Ni-NTA complexes presented on the surface of the particle could capture His_6-tagged proteins through strong affinity binding. The conjugated proteins mCherry and eGFP were within close proximity and a FRET effect between them was detected. The catalytic activity of assembled cellulases was elevated by more than twofold after assembly with Ni-NTA-containing micelles; this could be attributed to an enhanced local concentration and the synergy effect.

Experimental Section

Assembly of PS-*b*-PSMANi-NTA with different proteins: The synthetic procedures for the preparation of PS-*b*-PSMANi-NTA micelles, and the expression and purification steps of eGFP, mCherry, and cellulases are described in the Supporting Information. The concentration of Ni-NTA moieties in the prepared micelle was about 0.82 mM. Based on this concentration, the number of moles of protein assembled with the micelle was also calculated. The molar ratio of Ni-NTA to fluorescent protein was 10:1, and the molar ratios of Ni-NTA to cellulases were fixed at 0:1, 5:1, 10:1, and 20:1, respectively. The buffer for the assembly process was pH 8.0, 50 mM Tris·HCl buffer, unless otherwise stated. Various concentrations of micelles were prepared, and the protein solution was then added and gently mixed. The mixture was incubated at 4 °C and assembled overnight.

FRET tests of PS-*b*-PSMANi-NTA–mCherry–eGFP and PS-*b*-PSMANi-NTA–eGFP: mCherry and eGFP were assembled with PS-b-PSMANi-NTA. The molar ratio of Ni-NTA to protein was 10:1, and the molar ratio of mCherry to eGFP was controlled at 1:1. The PS-*b*-PSMANi-NTA–eGFP assembly was prepared as a control. The particles were centrifuged for 10 min at 9000 rcf for separation from the assembled suspension, then resuspended in pure water. The particles were dispersed on a precleaned glass plate, covered by a coverslip, and sealed with nail polish. The coverslip and plates were first soaked in a 10:1 (*v*/*v*) mixture of concentrated H_2SO_4 and 30% H_2O_2 overnight, extensively rinsed with water, sonicated in absolute ethanol for 10 min, and dried with a stream of air. The fluorescence measurement system included a self-assembled confocal microscope with an oil immersion 60× NA1.4 and PlanApo objective lens (Olympus), a continuous-wave laser (405 nm, 100 μW), filter cubes/sets, and two photomultiplier tubes (PMTs; HAMAMATSU, R-928).

Enzymatic activity assay: Cellulose hydrolysis reactions were performed in Tris·HCl buffer (50 mM, pH 8.0) with 0.1% PASC. Reactions were performed at 37 °C and samples (200 μL) were collected periodically and immediately mixed with DNS reagents (600 μL; 10 g L^{-1} dinitrosalicylic acid, 10 g L^{-1} sodium hydroxide, 2 g L^{-1} phenol, 0.5 g L^{-1} sodium sulfite). After incubation at 95 °C for 10 min, 40% Rochelle salts (200 μL; potassium sodium tartrate) was added to fix the color before the UV/Vis absorbance of the supernatants was read at $\lambda = 575$ nm.

Acknowledgements

We gratefully acknowledge financial support from the NSF and SC EPSCoR/IDeA Program under NSF Award #OIA-1655740. The views, perspectives, and content do not necessarily represent the official views of the SC EPSCoR/IDeA Program nor those of the NSF.

Conflict of Interest

The authors declare no conflict of interest.

Keywords: immobilization · micelles · polymers · proteins · self-assembly

[1] E. A. Bayer, E. Morag, R. Lamed, *Trends Biotechnol.* **1994**, *12*, 379–386.
[2] a) E. A. Bayer, J.-P. Belaich, Y. Shoham, R. Lamed, *Annu. Rev. Microbiol.* **2004**, *58*, 521–554; b) L. Viikari, J. Vehmaanperä, A. Koivula, *Biomass Bioenergy* **2012**, *46*, 13–24.
[3] a) H.-P. Fierobe, A. Mechaly, C. Tardif, A. Belaich, R. Lamed, Y. Shoham, J.-P. Belaich, E. A. Bayer, *J. Biol. Chem.* **2001**, *276*, 21257–21261; b) H.-P. Fierobe, E. A. Bayer, C. Tardif, M. Czjzek, A. Mechaly, A. Bélaich, R. Lamed, Y. Shoham, J.-P. Bélaich, *J. Biol. Chem.* **2002**, *277*, 49621–49630.
[4] a) S.-L. Tsai, J. Oh, S. Singh, R. Chen, W. Chen, *Appl. Environ. Microbiol.* **2009**, *75*, 6087–6093; b) S.-L. Tsai, G. Goyal, W. Chen, *Appl. Environ. Microbiol.* **2010**, *76*, 7514–7520; c) F. Wen, J. Sun, H. Zhao, *Appl. Environ. Microbiol.* **2010**, *76*, 1251–1260.
[5] a) Q. Sun, B. Madan, S.-L. Tsai, M. P. DeLisa, W. Chen, *Chem. Commun.* **2014**, *50*, 1423–1425; b) Q. Sun, W. Chen, *Chem. Commun.* **2016**, *52*, 6701–6704.
[6] S. L. Tsai, M. Park, W. Chen, *Biotechnol. J.* **2013**, *8*, 257–261.
[7] Y. Zhang, Y. Yang, W. Ma, J. Guo, Y. Lin, C. Wang, *ACS Appl. Mater. Interfaces* **2013**, *5*, 2626–2633.
[8] a) G. N. Grover, H. D. Maynard, *Curr. Opin. Chem. Biol.* **2010**, *14*, 818–827; b) P. Thordarson, B. Le Droumaguet, K. Velonia, *Appl. Microbiol. Biotechnol.* **2006**, *73*, 243.
[9] a) Z. Gu, T. T. Dang, M. Ma, B. C. Tang, H. Cheng, S. Jiang, Y. Dong, Y. Zhang, D. G. Anderson, *ACS Nano* **2013**, *7*, 6758–6766; b) W. Fan, L. Liu, H. Zhao, *Angew. Chem. Int. Ed.* **2017**, *56*, 8844–8848; *Angew. Chem.* **2017**, *129*, 8970–8974; c) Z. Sun, U. Glebe, H. Charan, A. Böker, C. Wu, *Angew. Chem. Int. Ed.* **2018**, *57*, 13810–13814; *Angew. Chem.* **2018**, *130*, 14006–14010.
[10] a) J. Nicolas, S. Mura, D. Brambilla, N. Mackiewicz, P. Couvreur, *Chem. Soc. Rev.* **2013**, *42*, 1147–1235; b) V. Postupalenko, D. Desplancq, I. Orlov, Y. Arntz, D. Spehner, Y. Mely, B. P. Klaholz, P. Schultz, E. Weiss, G. Zuber, *Angew. Chem. Int. Ed.* **2015**, *54*, 10583–10586; *Angew. Chem.* **2015**, *127*, 10729–10732; c) C. Ju, R. Mo, J. Xue, L. Zhang, Z. Zhao, L. Xue, Q. Ping, C. Zhang, *Angew. Chem. Int. Ed.* **2014**, *53*, 6253–6258; *Angew. Chem.* **2014**, *126*, 6367–6372.
[11] a) T. Li, L. Wu, N. Suthiwangcharoen, M. A. Bruckman, D. Cash, J. S. Hudson, S. Ghoshroy, Q. Wang, *Chem. Commun.* **2009**, 2869–2871; b) N. Suthiwangcharoen, T. Li, L. Wu, H. B. Reno, P. Thompson, Q. Wang, *Biomacromolecules* **2014**, *15*, 948–956; c) L. Zhang, Y. Xu, T. M. Makris, Q. Wang, *Biomacromolecules* **2018**, *19*, 918–925; d) L. Lu, L. Yuan, J. Yan, C. Tang, Q. Wang, *Biomacromolecules* **2016**, *17*, 2321–2328; e) X. Zhang, X. Zhao, J. A. Luckanagul, J. Yan, Y. Nie, L. A. Lee, Q. Wang, *ACS Macro Lett.* **2017**, *6*, 442–446.
[12] a) M.-Q. Zhu, L.-H. Wei, M. Li, L. Jiang, F.-S. Du, Z.-C. Li, F.-M. Li, *Chem. Commun.* **2001**, 365–366; b) M. P. Baranello, L. Bauer, D. S. Benoit, *Biomacromolecules* **2014**, *15*, 2629–2641.
[13] S. Harrisson, K. L. Wooley, *Chem. Commun.* **2005**, 3259–3261.

[14] a) D. W. Piston, G.-J. Kremers, *Trends Biochem. Sci.* **2007**, *32*, 407–414; b) K. Truong, M. Ikura, *Curr. Opin. Struct. Biol.* **2001**, *11*, 573–578; c) H. Wallrabe, A. Periasamy, *Curr. Opin. Biotechnol.* **2005**, *16*, 19–27.
[15] C. S. Walseth, *Tappi* **1952**, *35*, 228–233.
[16] G. L. Miller, *Anal. Chem.* **1959**, *31*, 426–428.
[17] a) M. Z. Li, S. J. Elledge, *Nat. Methods* **2007**, *4*, 251; b) L. Artzi, E. A. Bayer, S. Moraïs, *Nat. Rev. Microbiol.* **2017**, *15*, 83.

Manuscript received: January 28, 2019
Accepted manuscript online: January 29, 2019
Version of record online: April 15, 2019